RSC Advances

PAPER

View Article Online
View Journal | View Issue



Cite this: *RSC Adv.*, 2018, **8**, 38681

# Enhanced mechanical, thermal, and UV-shielding properties of poly(vinyl alcohol)/metal–organic framework nanocomposites

Yibo Dai,†[a] Qun Tang,†[a] Ziang Zhang,[a] Caili Yu,[a] Heping Li,[a] Lin Xu,*[b] Shufen Zhang[ac] and Zhiming Zou*[a]

Received 27th August 2018
Accepted 12th November 2018

DOI: 10.1039/c8ra07143h

rsc.li/rsc-advances

Metal–organic framework (HKUST-1) nanoparticles were successfully synthesized, and poly(vinyl alcohol) (PVA)/HKUST-1 nanocomposite films were fabricated by a simple solution casting method. Our results showed that the addition of HKUST-1 caused a remarkable enhancement in both thermal stability and mechanical properties of the PVA nanocomposites, due to the homogeneous distribution of HKUST-1 and the strong interfacial interactions between PVA and HKUST-1. With incorporation of 2 wt% HKUST-1, the degradation temperature of the nanocomposites was about 33 °C higher than that of pure PVA. At the same time, the Young's modulus and tensile strength of the nanocomposites was approximately 137% and 32% higher than those of pure PVA, respectively. Moreover, the PVA/HKUST-1 nanocomposites also showed strikingly enhanced UV-shielding ability as well as satisfactory visible light transmittance, which revealed that HKUST-1 nanoparticles could act as a good UV absorber in nanocomposites. This work provides a novel and simple method for producing UV-shielding materials with simultaneously enhanced thermal and mechanical properties, which have potential applications in UV protection areas.



## 1. Introduction

Since the first major success in exfoliation of montmorillonite in nylon-6 and fabrication of nanocomposites with significant enhancements in the tensile strength and Young's modulus,[1] numerous polymer nanocomposites have been developed through incorporating various nanofillers (*e.g.*, carbon nanotubes,[2,3] graphene,[4,5] clay,[6] silica,[7] titania,[8] nanorods,[9] nanodiamond,[10] *etc.*) into a range of polymers. The incorporated nanofillers were reported to upgrade and diversify polymer materials properties such as excellent mechanical strength and toughness,[11,12] high thermal stability,[13] low water/gas permeability,[14,15] good optical features,[16–18] flame retardancy[19] ultraviolet (UV)-shielding[20] and dielectric properties.[21]

Metal–organic frameworks (MOFs) are a class of crystalline porous materials with periodic network structures that are usually formed by self-assembly of inorganic metal centers (metal ions or metal clusters) and organic ligands. MOFs nanoparticles have received broad attention due to their high specific surface area, tunable functionalities and convenient synthesis, making them being used widely in gas storage and separation,[22] magnetic refrigeration,[23] sensing,[24] catalysis,[25] proton conduction,[26,27] and biomedical imaging.[28] Moreover, MOFs nanoparticles possess high thermal stability, and good affinity with polymer chains arose from the strong interaction between the organic ligands in MOFs and polymer chains.[29,30] Thus, it can be expected an effective dispersion of MOFs nanoparticles into polymers and resins, which is crucial for the preparation and properties of polymer nanocomposites. To date, ongoing efforts are focused on using MOFs nanoparticles as functional fillers to construct novel polymer nanocomposites. For example, Shi *et al.*[31] showed that incorporating MOFs (ZIF-8) nanoparticles into poly(lactic acid) (PLA) by solution-blending method could improve the mechanical, flame retardant, and dielectric properties of PLA nanocomposites. Hou *et al.*[32] investigated the thermal and flame retardant properties of the polystyrene (PS)/Fe-MOF and PS/Co-MOF nanocomposite films. The results showed that both the thermostability and flame retardancy were significantly enhanced by the incorporated Fe-MOF or Co-MOF nanoparticles. Liu *et al.*[33] investigated the biocompatibility and antibacterial properties of the poly(ε-caprolactone) (PCL)/Zr-MOF nanocomposites. The prepared nanocomposites had good biocompatibility and antibacterial ability. E. D. Dikio *et al.*[34] reported the fabrication of novel PVA/MOF nanofibers, which displayed higher potential removal of Pb(II) ions than neat PVA nanofibres. Among the several physicochemical

[a]*Guangxi Key Laboratory of Electrochemical and Magnetochemical Functional Materials, College of Chemistry and Bioengineering, Guilin University of Technology, Guilin 541004, China. E-mail: 2014005@glut.edu.cn*

[b]*Laboratory of Surface Physics and Chemistry, Guizhou Education University, Guiyang 550018, China. E-mail: lxu@gznc.edu.cn*

[c]*State Key Laboratory of Fine Chemicals, Dalian University of Technology, Dalian 116024, P. R. China*

† The authors contributed equally to this work.

properties of polymer nanocomposites, the shielding against UV-light allows very special applications. Specifically, prolonged exposure to UV-light can cause severe negative effects in dyes, pigments, semiconductor devices, and polymeric materials.[35] In this context, many efforts have been devoted to developing polymer composites with UV-shielding properties, including applications such as optical filters and protective UV coatings.[36,37] Nevertheless, the impacts of MOF nanoparticles on mechanical, thermal, and UV-shielding properties of polymer composites have not yet been evaluated systematically.

Poly(vinyl alcohol) (PVA), as a kind of water-soluble and biodegradable polymer, has been widely used not only in scientific fields but also in industrial fields.[10] PVA possesses excellent chemical stability, film formation, adhesive and mechanical properties, low cost and widespread application, making it a modal matrix for the research of polymer composites. In this study, copper-based MOF (HKUST-1) nanoparticles were synthesized and applied as UV absorber in nanocomposites for the first time. PVA was selected as a polymer matrix and blended with HKUST-1 by a solution method to prepare the PVA/HKUST-1 nanocomposites. As shown in Scheme 1, since there exist a great number of oxygen-containing functional groups on the surface of HKUST-1 nanoparticles as well as hydroxy groups in the PVA molecules, it will facilitate the formation of a hydrogen bond between HKUST-1 and PVA, and thus the effective dispersion of HKUST-1 nanoparticles in the nanocomposites. In addition, not only the mechanical and thermal properties, but also the UV-shielding capability of the nanocomposites has been strikingly enhanced with the incorporation of HKUST-1.

## 2. Experimental section

### 2.1. Materials

Polyvinyl alcohol (PVA-210, $M_w$ = 67 000) was purchased from Aladdin Industrial Corporation (Shanghai, China). Analytical grade reagents copper nitrate ($Cu(NO_3)_2 \cdot 3H_2O$), triethylamine ($Et_3N$) and ethanol were supplied by Xilong Scientific Co. (China). Benzene-1,3,5-tricarboxylic acid ($C_9H_6O_6$, BTC) was purchased from HWRK Chemical Co. (Beijing, China). All the reagents were used as received.

### 2.2. Synthesis of HKUST-1 nanoparticles

HKUST-1 nanoparticles were synthesized according to the literature.[38] 10 mmol $Cu(NO_3)_2 \cdot 3H_2O$ was dissolved in 100 mL deionized water. Separately, 10 mmol BTC and 1.4 mL $Et_3N$ were also dissolved in 100 mL deionized water. Then 1.5 mL of the prepared $Cu(NO_3)_2$ aqueous solution and 1 mL of the prepared BTC–$Et_3N$ aqueous solution were respectively added into 50 mL of 1 : 1 (v/v) mixture of deionized water and ethanol with magnetic stirring, and the reaction mixture was stirred for 1 h at room temperature. The obtained blue powder was centrifuged, washed with ethanol for 3 times, and then dried under vacuum for 5 h at room temperature.

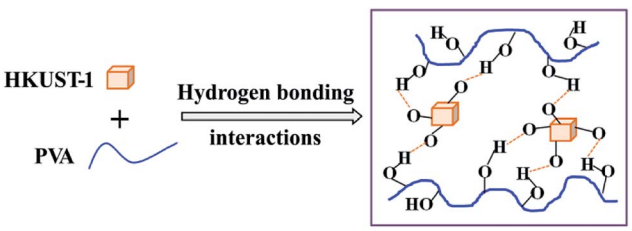


Scheme 1 Schematic illustration of the interactions between HKUST-1 PVA.

### 2.3. Preparation of the PVA/HKUST-1 nanocomposites

PVA/HKUST-1 nanocomposite films were fabricated by a simple casting method. First, 1.5 g PVA was dissolved in 13.5 mL deionized water by heating to 90 °C for 2 h to prepare a 10 wt% PVA solution. Simultaneously, the desired amount of HKUST-1 (7.5; 15; and 30 mg) was dispersed in 4 mL ethanol under ultrasonic irradiation (40 kHz, 300 W) for 30 min. Subsequently, the HKUST-1 suspension in ethanol was slowly added dropwise into the PVA solution and stirred for another 1 h. Next, the obtained PVA/HKUST-1 film-forming solution was slowly cast onto a glass plate (125 mm × 125 mm × 15 mm) placed horizontally, and dried at ambient temperature for 5 days. Finally, the PVA/HKUST-1 films were peeled off the substrate and then dried in a vacuum at 40 °C for 48 h to constant weight. The thickness of the films was controlled at ~60 μm by casting the same amount (12 mL) of film-forming solution per plate. The HKUST-1 content in the composites was 0.5; 1.0; and 2.0 wt% in relation to PVA weight, resulting in PVA-0.5, PVA-1.0, and PVA-2.0 samples, respectively. PVA films (without any HKUST-1) were prepared as a control.

### 2.4. Characterization

X-ray diffraction (XRD) patterns were measured by Bruker D8 Advance diffractometer at 40 kV and 40 mA with Cu Kα radiation. Fourier transform infrared (FTIR) spectra were measured on a Nicolet NEXUS-470 infrared spectrophotometer using the KBr method. The morphologies of HKUST-1 and the fracture surfaces of PVA/HKUST-1 nanocomposites were observed using a field emission scanning electron microscope (SEM) (SU-5000, Hitachi) coupled with an energy dispersive X-ray (EDX) spectrometer. Differential scanning calorimetry (DSC) measurements were carried out under dry nitrogen by a TA Q200 apparatus (TA Instruments), from 30 to 220 °C at 10 °C $min^{-1}$. The crystallinity ($X_c$) of all samples was calculated as $X_c = \Delta H_m / \Delta H_0(1 - \omega)$, where $\Delta H_m$ is the measured melting enthalpy from DSC, $\Delta H_0$ is the melting enthalpy of the 100% PVA crystalline (138.6 J $g^{-1}$)[39,40] and $\omega$ the weight fraction of HKUST-1 in the composites. Thermogravimetric analysis (TGA) was performed with a thermal analyzer, Perkin-Elmer TGA7 (ITK Co., Ltd.), at a heating rate of 10 °C $min^{-1}$ and under nitrogen flow. Ultraviolet-visible (UV-vis) spectra were observed with a TU-1901 UV-vis spectrophotometer from 200 to 800 nm. All the above mentioned measurements were performed on three samples of each formulation, and the reported results are average values.

Tensile testing measurements were carried out on an Instron 1121 machine with the crosshead rate of 10 mm $min^{-1}$ at room

 

temperature according to ASTM D638. At least five samples of each formulation were tested from which the mean and standard deviation were calculated.

## 3. Results and discussions

### 3.1. Characterization of HKUST-1

The representative XRD pattern of HKUST-1 nanoparticles is shown in Fig. 1a. All the characteristic diffraction peaks are consistent with previous reports,[38,41] confirming that the synthesized HKUST-1 nanoparticles are pure phase. Moreover, one sharp and intense peak at about $2\theta = 11.6^{\circ}$ can be observed, which suggests high crystallinity for the synthesized HKUST-1 nanoparticles.[38] Fig. 1b shows the SEM image of HKUST-1 nanoparticles. It can be seen that the synthesized HKUST-1 nanoparticles are roughly cubic in shape, with particle sizes of approximately 100–200 nm.

### 3.2. Dispersion of HKUST-1 nanoparticles into PVA

To study the dispersion of HKUST-1 nanoparticles in the PVA matrix, the morphology and structure of PVA/HKUST-1 nanocomposite films were observed by SEM. Fig. 2a shows the cross-sectional SEM image of the PVA/HKUST-1 nanocomposite film containing 2.0 wt% HKUST-1. It can be clearly seen that the HKUST-1 nanoparticles are well-embedded and uniformly dispersed in the PVA matrix without obvious agglomeration. Fig. 2b and c exhibits the EDX mapping images of C and Cu, respectively, demonstrating their homogeneous distribution. This result further confirms the well dispersion of HKUST-1 nanoparticles in the PVA/HKUST-1 nanocomposite. Such excellent dispersion could be due to the good interfacial compatibility between HKUST-1 and PVA, and similar results were observed for the PLA/ZIF-8 nanocomposites,[31] which suggested a strong interaction between the filler and the matrix polymer.

Accordingly, FTIR tests were carried out to illuminate the interaction between HKUST-1 and PVA. Fig. 3 shows the FTIR absorption spectra of neat PVA and PVA/HKUST-1 nanocomposites. For pure PVA, the wide absorption band at about 3347 $cm^{-1}$ is arised from O–H stretching vibration of hydroxyl group, which is sensitive to the hydrogen bond. With regard to PVA/HKUST-1 films, the hydroxyl (O–H) peak at 3347 $cm^{-1}$ gradually shifts to higher wavenumbers with increasing HKUST-1 content, and an approximately 14 $cm^{-1}$ blue shift can be observed for PVA-2.0 film containing 2.0 wt% HKUST-1. This upward shifting also suggests that there exist strong interactions between HKUST-1 and PVA, which agree well with the SEM results. The strong interactions at the filler–matrix interface are mainly ascribed to the new hydrogen bonding formed between the oxygen-containing functional groups on the surface of HKUST-1 and the hydroxyl groups of PVA chains (Scheme 1).

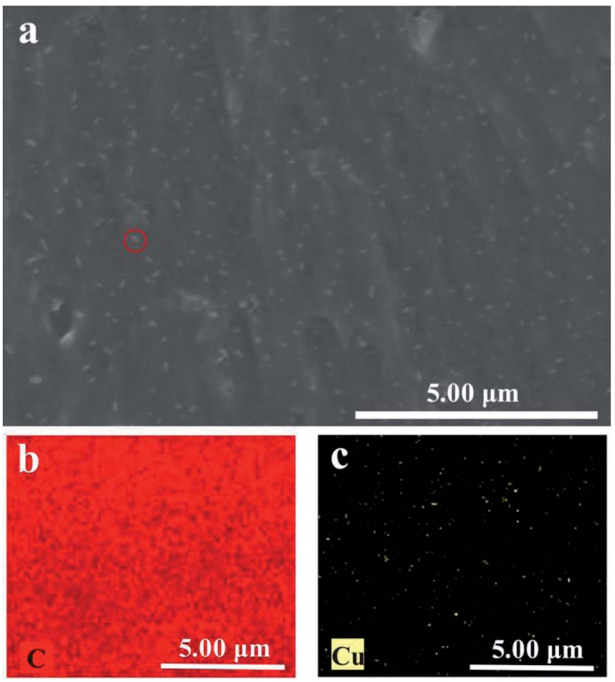


Fig. 2 SEM image (a) and the EDX elemental mapping images for (b) C and (c) Cu of PVA-2.0 nanocomposite.

### 3.3. Thermal properties of PVA/HKUST-1 nanocomposites

To understand the effect of HKUST-1 on the properties of the matrix polymer, the thermal stability of PVA and PVA/HKUST-1 nanocomposites was examined by TGA with a nitrogen

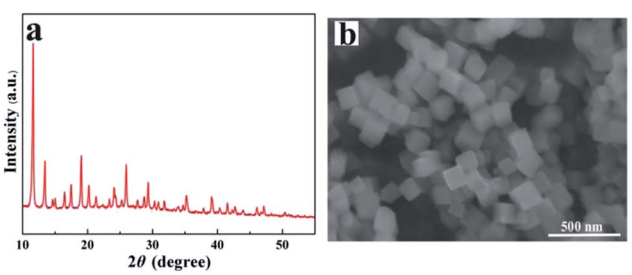


Fig. 1 XRD pattern (a) and SEM image (b) for HKUST-1.

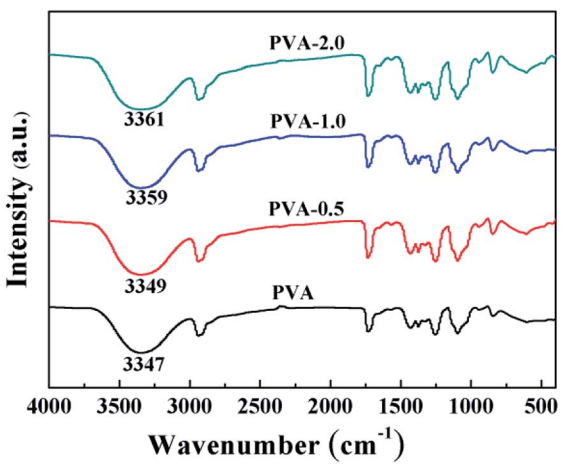


Fig. 3 FTIR spectra of PVA and PVA/HKUST-1 nanocomposite films.

atmosphere, and the TGA and relevant DTG curves are demonstrated in Fig. 4. It can be found that all the samples of pure PVA and its nanocomposites show a three-step weight loss process, including (a) the initial weight loss occurring at about 60–150 °C, which is ascribed to the evaporation of the residual (or absorbed) solvent; (b) the second stage observed at about 200–350 °C, which is mainly due to the thermal decomposition of side chains of PVA; (c) the third weight loss at around 400–450 °C, which can be related to the decomposition of the main chains of PVA. These results are in accordance with similar studies of Zhang *et al.*[42] reported in literature. Quantitatively, the incorporation of HKUST-1 into the PVA matrix results in a higher thermal stability of the composite films, as evaluated from the onset decomposition temperature ($T_{onset}$) and the maximum decomposition temperature ($T_{max1}$ and $T_{max2}$) (Table 1). For instance, the $T_{onset}$, $T_{max1}$ and $T_{max2}$ of neat PVA are 262, 320 and 421 °C, respectively, whereas with the addition of 2.0 wt% HKUST-1, $T_{onset}$, $T_{max1}$ and $T_{max2}$ increase to 295, 329 and 438 °C, respectively, the $T_{onset}$ of which is about 33 °C higher than that of neat PVA. The remarkable enhancement in thermal stability could probably be ascribed to the strong interfacial interactions between HKUST-1 and PVA, which impedes the elimination and oxidization of side hydroxyl groups of PVA, thus causing a significant suppression of the thermal degradation process.[39,43]

The thermal properties of PVA/HKUST-1 nanocomposites can also be characterized by DSC measurement, as shown in Fig. 5 and in Table 1. The glass transition temperatures ($T_g$) for pure PVA, PVA-0.5, PVA-1.0, and PVA-2.0 films are 68.5, 69.6, 70.8, and 71.2 °C, respectively (Table 1), indicating a moderate shift toward a higher $T_g$ with increasing HKUST-1 content. The increase in $T_g$ could be due to the strong hydrogen bonding interactions between HKUST-1 and PVA matrix and the rigidity of the HKUST-1 itself, which would constrain the mobility of the PVA chains.[44] Furthermore, the $\Delta H_m$ of PVA/HKUST-1 nanocomposites achieved from second heating process is distinctly increased as compared with that of neat PVA, and the crystallization degree ($X_c$) of PVA/HKUST-1 nanocomposites also increases from 17.4% to 30.3% as the HKUST-1 content increased from 0 wt% to 2.0 wt%. This indicates that the HKUST-1 can act as a nucleation agent and promote crystallization of PVA; thus, the $X_c$ can be improved by the incorporation of the HKUST-1 nanoparticles. Meanwhile, the melting temperature ($T_m$) of PVA/HKUST-1 nanocomposites is higher than that of pure PVA and increases with the increasing loading of HKUST-1. The significant increase in $T_m$ can be related to the ordered arrangement of PVA chains induced by HKUST-1 nanoparticles and the enhanced crystallization degree of PVA/HKUST-1 to some extent.

### 3.4. Mechanical properties of PVA/HKUST-1 nanocomposites

Based on the strong interfacial adhesion between the components, and the improved crystallinity of PVA, the mechanical performance of PVA/HKUST-1 nanocomposites was expected to be significantly enhanced by the well dispersed HKUST-1 nanoparticles. To verify this, the tensile tests were carried out to investigate the mechanical properties of PVA/HKUST-1 films. Fig. 6a shows the typical stress–strain curves of neat PVA and PVA/HKUST-1 nanocomposite films. Compared with pure PVA, PVA/HKUST-1 nanocomposites obviously exhibit higher Young's modulus ($E$) and tensile strength ($\sigma$), but accompanying the slightly decreasing of elongation at break, which can be often observed in other filler-reinforced polymer composites.[10,32,44–47] Fig. 6b represents the relationships between the $E$, the $\sigma$, and the HKUST-1 content of the PVA/HKUST-1 nanocomposites. It is observed in Fig. 6b that the $E$ and $\sigma$ of PVA/HKUST-1 nanocomposites have a monotonous increasing tendency with the increase of the HKUST-1 content. For instance, the $E$ and $\sigma$ of neat PVA are 0.43 GPa and 25.1 MPa, respectively. With the addition of 0.5 wt% HKUST-1, the $E$ and $\sigma$ increase to 0.58 GPa and 28.5 MPa, respectively. As further increasing HKUST-1 content to 2.0 wt%, the $E$ and $\sigma$ is raised to 1.02 GPa and 33.2 MPa, respectively, which is approximately 137% and 32% higher than those of neat PVA film. The remarkable improvement in $E$ and $\sigma$ suggests that HKUST-1 nanoparticle is a very effective reinforcing agent for PVA matrix. HKUST-1 has an unique surface structure and high surface area, making possible the effective absorption and dispersion of impact energy.[31,39] Moreover, the well-dispersed HKUST-1 nanoparticles in PVA matrix and the strong interfacial interactions between PVA and HKUST-1, as shown in Scheme 1, not only can inhibit phase separation, but also

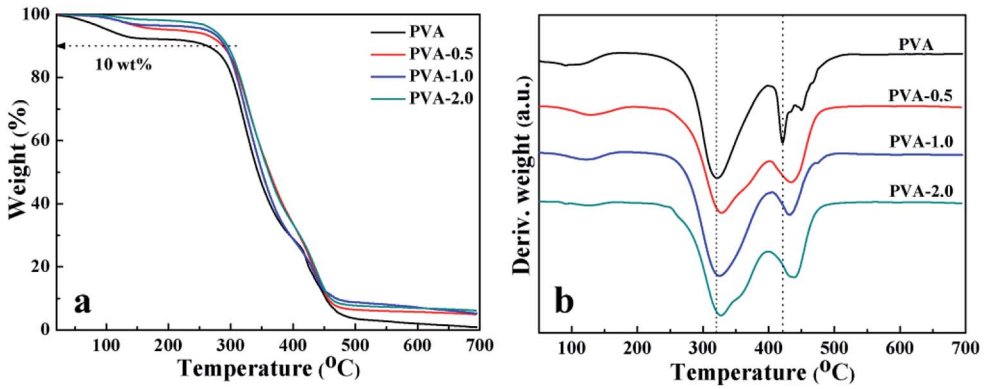


Fig. 4 (a) TGA and (b) DTG curves of neat PVA and PVA/HKUST-1 nanocomposites.

Table 1 The onset decomposition temperature ($T_{onset}$) and the max thermal decomposition temperatures of first stage and second stage ($T_{max1}$ and $T_{max2}$) for neat PVA and PVA/HKUST-1 films. Glass transition temperatures ($T_g$), melting temperatures ($T_m$), melting enthalpies ($\Delta H_m$) and crystallinity ($X_c$) of the films[a]

| | TGA | | | DSC | | | |
|---|---|---|---|---|---|---|---|
| Sample | $T_{onset}$ (°C) | $T_{max1}$ (°C) | $T_{max2}$ (°C) | $T_g$ (°C) | $T_m$ (°C) | $\Delta H_m$ (J g$^{-1}$) | $X_c$ (%) |
| PVA | 262 ± 3 | 320 ± 2 | 421 ± 4 | 68.5 ± 0.2 | 173.4 ± 0.5 | 24.2 ± 0.4 | 17.4 ± 0.3 |
| PVA-0.5 | 287 ± 2 | 329 ± 3 | 433 ± 3 | 69.6 ± 0.1 | 185.5 ± 0.4 | 32.9 ± 0.5 | 23.8 ± 0.4 |
| PVA-1.0 | 291 ± 1 | 327 ± 2 | 433 ± 3 | 70.8 ± 0.1 | 187.7 ± 0.4 | 36.6 ± 0.3 | 26.4 ± 0.2 |
| PVA-2.0 | 295 ± 2 | 329 ± 1 | 438 ± 4 | 71.2 ± 0.2 | 196.2 ± 0.6 | 42.1 ± 0.5 | 30.3 ± 0.4 |

[a] Values were expressed as mean ± standard error.

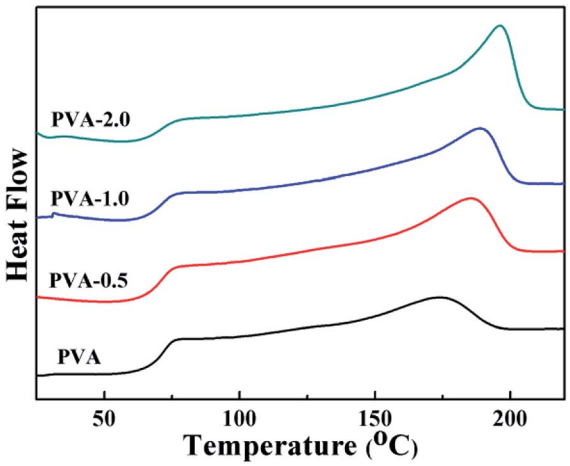


Fig. 5 DSC curves of neat PVA and PVA/HKUST-1 nanocomposites.

ensure an efficient load transfer at the interface. Besides the excellent reinforcing effect of HKUST-1 nanoparticles, the increased crystallinity $X_c$ of the PVA matrix induced by the HKUST-1 is also beneficial to improve the mechanical properties of the PVA/HKUST-1 nanocomposites. Therefore, the mechanical properties of PVA matrix can be remarkably improved even by a small amount of HKUST-1 nanoparticles.

### 3.5. UV-shielding performance of PVA/HKUST-1 films

UV radiation accounts for only 3% of the total solar radiation that penetrates the earth's surface, but it can cause chemical reactions, fading of certain coloring, weathering of polymers, and even eye and skin damage.[48] Therefore, UV light shielding is one of the most important properties of polymer materials exposed to UV light that determines their ultimate applications. Fig. 7a displays the optical photographs of neat PVA and PVA/HKUST-1 nanocomposites. It is obvious that the neat PVA film is colorless and highly transparent, whereas the PVA/HKUST-1 films are light blue due to the color of the HKUST-1, and their color gradually deepens with increased HKUST-1 content. Meanwhile, all PVA/HKUST-1 nanocomposite films are visually uniform and transparent. The optical properties of PVA and PVA/HKUST-1 nanocomposite films were characterized by UV-vis spectroscopy, as shown in Fig. 7b. For pure PVA film, the transmittance across the visible regions (400–800 nm) is higher than 86%. After incorporation of HKUST-1 into PVA, a gradual decrease in the transmittance of visible light can be observed for the PVA/HKUST-1 nanocomposite films. At the highest loading (2.0 wt%) of HKUST-1 used in this study, the transmittance at 550 nm for PVA-2.0 film is still up to 67%, revealing a slight decrease in the light transparency compared with that of the pure PVA film. The extraordinary optical transparency for the PVA/HKUST-1 films could be related to the well dispersion of the HKUST-1 in the PVA matrix (Fig. 2), which has few effects on the transmittance of the nanocomposites.

Moreover, it is noted that neat PVA film presents little absorbance in UV region from 200 to 400 nm, while a sharp absorption increasing in UV region is observed when HKUST-1 nanoparticles are incorporated into PVA film, even the content as low as 0.5 wt%. It demonstrates a promoted UV light

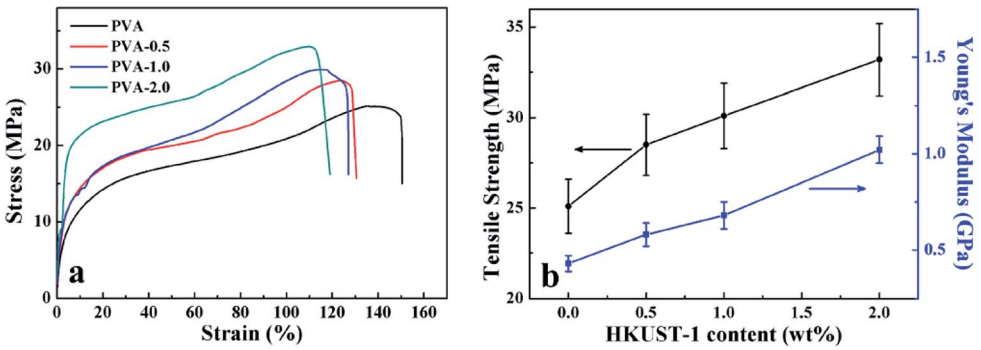


Fig. 6 (a) Representative stress–strain curves, (b) Young's modulus ($E$) and tensile strength ($\sigma$) of the neat PVA and PVA/HKUST-1 nanocomposites.

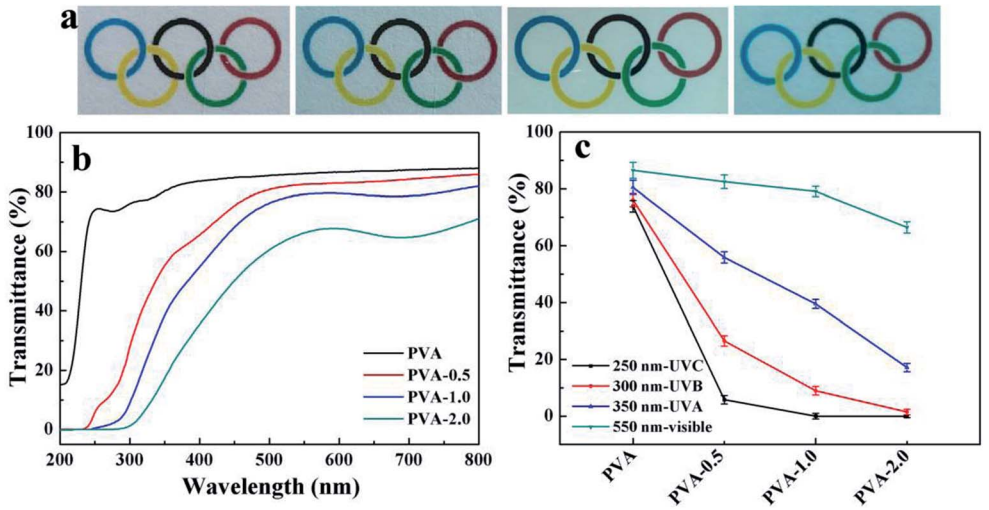


Fig. 7 (a) Photographs of neat PVA, PVA-0.5, PVA-1.0, and PVA-2.0 films (placed on the paper with colored rings), from left to right, respectively. (b) UV-vis spectra of neat PVA and PVA/HKUST-1 nanocomposite films. (c) Transmittance change at specific UV light wavelengths (UVA, UVB, UVC).

shielding capacity by HKUST-1 nanoparticles in the spectra of interest. For quantify the UV shielding performance, we investigated the transmittance at specific UV light wavelengths for pure PVA and PVA/HKUST-1 nanocomposite films, and results are shown in Fig. 7c. It shows the PVA/HKUST-1 nanocomposite films have good absorbance of UV light at 350 nm (UVA), 300 nm (UVB), and 250 nm (UVC), and compared to pure PVA film, PVA/HKUST-1 nanocomposite films can be considered as potential UV-shielding materials. For instance, PVA-2.0 film can shield about 100% UVC, 98% UVB, and 83% UVA, while pure PVA film shields only 26% UVC, 24% UVB, and 19% UVA. Therefore, incorporation of HKUST-1 into PVA film can be in favor of the absorption of UV light and results in a novel transparent material with excellent UV-shielding performance. The UV-shielding capability of the obtained PVA/HKUST-1 nanocomposite films is much comparable to that using other organic or inorganic UV-absorbers,[20,37,49] which demonstrates HKUST-1 can be used as an effective UV-absorber for fabrication of a transparent UV-shielding film.

The UV-shielding contribution for each type of nanoparticle varies and mainly depends on its geometric shape and chemical structure. The widely exploited nanoparticles as UV-absorbers include inorganic metal oxide nanoparticles[50] (*e.g.*, ZnO, $SiO_2$, $TiO_2$, and $Al_2O_3$), graphene oxide nanosheets[17] and melanin nanoparticles,[51,52] *etc.* In this work, it is interesting to observe that the incorporation of HKUST-1 nanoparticles obviously upgrades the UV-shielding property of PVA. There are two factors about enhancing the UV-shielding performance of PVA/HKUST-1 films: (a) the well-dispersed HKUST-1 nanoparticles in matrix, which can effectively absorb UV light and rapidly convert the photon energy of UV light into heat. (b) The strong hydrogen interaction at the interface between the HKUST-1 nanoparticles and PVA matrix, which facilitates the formation of a large interface and thus the inevitably scattering of UV light at the interface. Meanwhile, the unique porous structure and high surface area of the HKUST-1 nanoparticles is also beneficial to the reflection and absorption of UV light, so the UV-shielding property of PVA matrix can be remarkably improved by the added HKUST-1 nanoparticles. Correspondingly, the schematic illustration of the UV-shielding action of PVA/HKUST-1 nanocomposite films is displayed in Scheme 2. Remarkably, the use of HKUST-1 as UV-absorber can offer a range of advantages when compared with other nanoparticles. First, the geometric shape and size of HKUST-1 nanoparticles can be regulated easily, thus their UV-shielding capacity can eventually be modulated. Furthermore, the organic linkers in

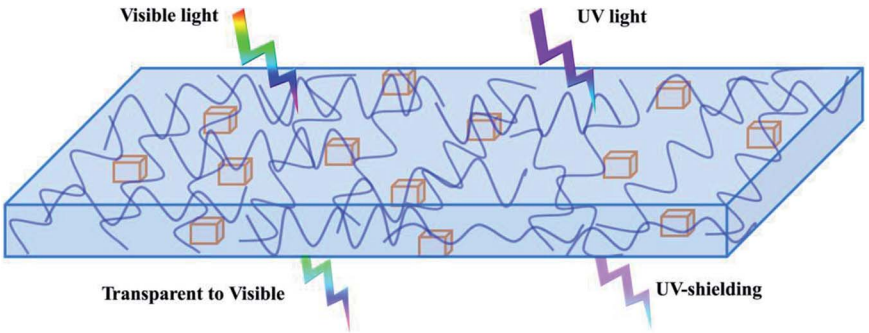


Scheme 2 Schematic illustration of the UV-shielding capacity of PVA/HKUST-1 nanocomposite films.

HKUST-1 nanoparticles allow them to interact with several types of polymers, thus resulting in nanocomposites with novel or enhanced properties. However, it should be noted that the photocatalytic activity of HKUST-1 nanoparticles is another important factor for assessing their potential applications in UV-shielding materials. Therefore, additional efforts are still needed to better understand the UV-shielding behavior in polymer nanocomposite materials based on HKUST-1.

## 4. Conclusions

Nano HKUST-1 particles were successfully prepared and then incorporated into PVA in an aqueous solution to fabricate PVA/HKUST-1 nanocomposites. The SEM micrographs confirmed the homogeneous dispersion of HKUST-1 nanoparticles in the PVA/HKUST-1 nanocomposites. Both the thermal stability and mechanical properties of the PVA/HKUST-1 nanocomposites were strikingly enhanced by the well-dispersed HKUST-1 nanoparticles. Moreover, PVA/HKUST-1 nano-composite films also exhibited a significant enhancement in UV-shielding capacity, combined with a satisfactory optical transparency at low HKUST-1 loading, which indicated HKUST-1 could act as a novel UV absorber in nanocomposite films. All in all, we created novel transparent nanocomposite films with excellent thermal stability, mechanical and UV-shielding properties by a simple and low-cost method, which could provide valuable insight into the rational design and fabrication of novel and excellent UV-shielding materials.

## Conflicts of interest

The authors declare no conflict of interest.

## Acknowledgements

This work was supported by the National Natural Science Foundation of China (21504018, 21466010, 21501033 and 51503048), the Natural Science Foundation of Guangxi Province (2016GXNSFBA380162, 2016GXNSFAA380062 and 2015GXNSFBA139024), the Natural Science Foundation of Guizhou Province (No. QKHJC[2017]1137), the Guangxi Key Laboratory of Electrochemical and Magnetochemical Functional Materials (EMFM20181122), and the special funding for distinguished expert from Guangxi Zhuang Autonomous Region.

## References

1 Y. Kojima, A. Usuki, M. Kawasumi, A. Okada, Y. Fukushima, T. Kurauchi and O. Kamigaito, *J. Mater. Res.*, 1993, **8**, 1185–1189.
2 K. Yusupov, A. Zakhidov, S. You, S. Stumpf, P. M. Martinez, A. Ishteev, A. Vomiero, V. Khovaylo and U. Schubert, *J. Alloys Compd.*, 2018, **741**, 392–397.
3 J. Liu, C. Chen, Y. Feng, Y. Liao, Y. Ye, X. Xie and Y.-W. Mai, *ACS Appl. Mater. Interfaces*, 2018, **10**, 1204–1216.
4 J. Ma, Y. Li, X. Yin, Y. Xu, J. Yue, J. Bao and T. Zhou, *RSC Adv.*, 2016, **6**, 49448–49458.
5 N. Wang, P. R. Chang, P. Zheng and X. Ma, *Appl. Surf. Sci.*, 2014, **314**, 815–821.
6 X. Su, S. Mahalingam, M. Edirisinghe and B. Chen, *ACS Appl. Mater. Interfaces*, 2017, **9**, 22223–22234.
7 L. Song, Z. Wang, X. Tang, L. Chen, P. Chen, Q. Yuan and L. Li, *Macromolecules*, 2017, **50**, 7249–7257.
8 S. Javadi, M. Panahi-Sarmad and M. Razzaghi-Kashani, *Polymer*, 2018, **145**, 31–40.
9 J. Sapkota, A. Shirole, E. J. Foster, J. C. Martinez Garcia, M. Lattuada and C. Weder, *Polymer*, 2017, **110**, 284–291.
10 S. Morimune, M. Kotera, T. Nishino, K. Goto and K. Hata, *Macromolecules*, 2011, **44**, 4415–4421.
11 J. C. Natterodt, J. Sapkota, E. J. Foster and C. Weder, *Biomacromolecules*, 2017, **18**, 517–525.
12 H. Ren, Y. Zhou, M. He, R. Xu, B. Ding, X. Zhong, Y. Tong, L. Fan, Z. Cai and H. Shen, *New J. Chem.*, 2018, **42**, 3069–3077.
13 S. Kumar, Sarita, M. Nehra, N. Dilbaghi, K. Tankeshwar and K.-H. Kim, *Prog. Polym. Sci.*, 2018, **80**, 1–38.
14 J. Ma, J. Pan, J. Yue, Y. Xu and J. Bao, *Appl. Surf. Sci.*, 2018, **427**, 428–436.
15 A. M. Youssef and S. M. El-Sayed, *Carbohydr. Polym.*, 2018, **193**, 19–27.
16 A. M. El-Nahrawy, A. I. Ali, A. B. A. Hammad and A. M. Youssef, *Int. J. Biol. Macromol.*, 2016, **93**, 267–275.
17 S. Xie, J. Zhao, B. Zhang, Z. Wang, H. Ma, C. Yu, M. Yu, L. Li and J. Li, *ACS Appl. Mater. Interfaces*, 2015, **7**, 17558–17564.
18 P. Singh, K. Mondal and A. Sharma, *J. Colloid Interface Sci.*, 2013, **394**, 208–215.
19 Y. Zhang, X. Zeng, X. Lai and H. Li, *RSC Adv.*, 2018, **8**, 111–121.
20 Y. Wang, X. Wang, T. Li, P. Ma, S. Zhang, M. Du, W. Dong, Y. Xie and M. Chen, *ACS Appl. Mater. Interfaces*, 2018, **10**, 13100–13106.
21 S. K. Kumar, B. C. Benicewicz, R. A. Vaia and K. I. Winey, *Macromolecules*, 2017, **50**, 714–731.
22 A. U. Czaja, N. Trukhan and U. Müller, *Chem. Soc. Rev.*, 2009, **38**, 1284–1293.
23 Q. Tang, P.-F. Li, Z.-M. Zou, Z. Liu and S.-X. Liu, *J. Solid State Chem.*, 2017, **246**, 329–333.
24 H. Xu, Y. Xiao, X. Rao, Z. Dou, W. Li, Y. Cui, Z. Wang and G. Qian, *J. Alloys Compd.*, 2011, **509**, 2552–2554.
25 E. A. Hall, L. R. Redfern, M. H. Wang and K. A. Scheidt, *ACS Catal.*, 2016, **6**, 3248–3252.
26 Q. Tang, Y. Liu, S. Liu, D. He, J. Miao, X. Wang, G. Yang, Z. Shi and Z. Zheng, *J. Am. Chem. Soc.*, 2014, **136**, 12444–12449.
27 Q. Tang, Y.-L. Yang, N. Zhang, Z. Liu, S.-H. Zhang, F.-S. Tang, J.-Y. Hu, Y.-Z. Zheng and F.-P. Liang, *Inorg. Chem.*, 2018, **57**, 9020–9027.
28 H. Furukawa, K. E. Cordova, M. O'Keeffe and O. M. Yaghi, *Science*, 2013, **341**, 1230444.
29 A. Zirehpour, A. Rahimpour and M. Ulbricht, *J. Membr. Sci.*, 2017, **531**, 59–67.

30 A. Donnadio, R. Narducci, M. Casciola, F. Marmottini, R. D'Amato, M. Jazestani, H. Chiniforoshan and F. Costantino, *ACS Appl. Mater. Interfaces*, 2017, **9**, 42239–42246.
31 X. Shi, X. Dai, Y. Cao, J. Li, C. Huo and X. Wang, *Ind. Eng. Chem. Res.*, 2017, **56**, 3887–3894.
32 Y. Hou, W. Hu, Z. Gui and Y. Hu, *Ind. Eng. Chem. Res.*, 2017, **56**, 2036–2045.
33 M. Liu, L. Wang, X. Zheng and Z. Xie, *ACS Appl. Mater. Interfaces*, 2017, **9**, 41512–41520.
34 N. D. Shooto, C. W. Dikio, D. Wankasi, L. M. Sikhwivhilu, F. M. Mtunzi and E. D. Dikio, *Nanoscale Res. Lett.*, 2016, **11**, 414.
35 A. L. Andrady, H. S. Hamid and A. Torikai, *Photochem. Photobiol. Sci.*, 2003, **2**, 68.
36 H. Moustafa, D. Darwish, A. Youssef, S. Reda and A. El-Wakil, *Egypt. J. Chem.*, 2017, **61**, 23–32.
37 A. C. de Moraes, P. F. Andrade, A. F. de Faria, M. B. Simoes, F. C. Salomao, E. B. Barros, C. Goncalves Mdo and O. L. Alves, *Carbohydr. Polym.*, 2015, **123**, 217–227.
38 Q. Liu, L.-N. Jin and W.-Y. Sun, *Chem. Commun.*, 2012, **48**, 8814–8816.
39 Y. Guan, W. Li, Y. Zhang, Z. Shi, J. Tan, F. Wang and Y. Wang, *Compos. Sci. Technol.*, 2017, **144**, 193–201.
40 J. Liang, Y. Huang, L. Zhang, Y. Wang, Y. Ma, T. Guo and Y. Chen, *Adv. Funct. Mater.*, 2009, **19**, 2297–2302.
41 L. H. Wee, M. R. Lohe, N. Janssens, S. Kaskel and J. A. Martens, *J. Mater. Chem.*, 2012, **22**, 13742.
42 S. Zhang, P. Liu, X. Zhao and J. Xu, *Appl. Surf. Sci.*, 2017, **396**, 1098–1107.
43 H. K. Cheng, N. G. Sahoo, Y. P. Tan, Y. Pan, H. Bao, L. Li, S. H. Chan and J. Zhao, *ACS Appl. Mater. Interfaces*, 2012, **4**, 2387–2394.
44 L. Jiang, X.-P. Shen, J.-L. Wu and K.-C. Shen, *J. Appl. Polym. Sci.*, 2010, **118**, 275–279.
45 Y. Wang, Z. Wang, P. Ma, H. Bai, W. Dong, Y. Xie and M. Chen, *RSC Adv.*, 2015, **5**, 72691–72698.
46 X. Zhao, Q. Zhang, D. Chen and P. Lu, *Macromolecules*, 2010, **43**, 2357–2363.
47 Y. Liang, X. Zhou, Y. Liao, J. Wu, X. Xie and H. Zhou, *Polymer*, 2016, **91**, 89–97.
48 Y. Shu, P. Yin, J. Wang, B. Liang, H. Wang and L. Guo, *Ind. Eng. Chem. Res.*, 2014, **53**, 3820–3826.
49 J. R. C. Smirnov, M. E. Calvo and H. Míguez, *Adv. Funct. Mater.*, 2013, **23**, 2805–2811.
50 M. E. Calvo, J. R. C. Smirnov and H. Míguez, *J. Polym. Sci., Part B: Polym. Phys.*, 2012, **50**, 945–956.
51 Y. Wang, T. Li, P. Ma, H. Bai, Y. Xie, M. Chen and W. Dong, *ACS Sustainable Chem. Eng.*, 2016, **4**, 2252–2258.
52 L. Qing, L. Guangfu, T. Jun and X. Zushun, *Macromol. Mater. Eng.*, 2018, **303**, 1700407.